Proceedings of the
International Conference on Mechanical Engineering 2007
(ICME2007) 29- 31 December 2007, Dhaka, Bangladesh

ICME07-AM-51

DYNAMIC ANALYSIS OF PITCH PLANE RAILWAY VEHICLE-TRACK INTERACTIONS DUE TO WHEEL FLAT

Rajib Ul Alam Uzzal[1], Waiz Ahmed[2] and Subhash Rakheja[3]

[1,2,3] Department of Mechanical and Industrial Engineering, Concordia University, Montreal, Canada

ABSTRACT

With demands for increased load and speed, the issue of wheel flats and a strategy for in-time maintenance and replacement of defective wheels has become an important concern for heavy haul operators. In this study, an analytical model of the coupled vehicle-track system is developed by integrating a pitch plane model of the vehicle with a two-dimensional model of the flexible track comprising 3-layers together with a nonlinear rolling contact model. The validated model is utilized to investigate the characteristics of impact forces due to wheel flats and its effect on motions and forces transmitted to vehicle and track components. The results are analyzed to examine the sequence of events as the wheel flat enters the contact area. The significant influence of wheel flat on various components of vehicle and track system is investigated in terms of the wheel-rail impact loads as well as bearing, railpad, and ballast forces.

Keywords: Wheel flat, pitch plane vehicle model, wheel-rail impact, component force.

1. INTRODUCTION

The existence of defects in a railway wheel is one of the main sources of railway vehicle-track abnormal vibrations. Wheel flat is the most common type of wheel defect encountered by the railway industry. With the significant increase of train speed and axle load, the vibration of the coupled vehicle and track system due to wheel flat is further intensified. Furthermore, the presence of flat on the wheel may cause excessive impact force and repeated dynamic loads not only on the wheel and rail, but also to the entire vehicle and track components. A comprehensive study on the influence of wheel flat is thus necessary for prediction of the impact force generated at the interfaces of different components of vehicle-track system.

The dynamic interaction between the vehicle, the wheel, and the rail track systems has been the subject of extensive research in recent years. Many studies [1, 2, 3] have focused on the vibrations of a railway track under moving vehicles with wheel defects, and different theories and models have been presented on this issue. A detailed review in the area of railway vehicle dynamics featuring the historical survey of the dynamic models to study the vehicles-track interactions due to wheel defects at high frequency range have been presented by Knothe and Grassie [4]. In analysis of the coupled vehicle-track system, some of these studies [3, 5] have employed finite element method and some [6, 7, 8] have used modal analysis method. Two types of track models are generally employed in the study of vehicle-track interactions. Early track system studies considering rail as a discretely supported beam [1, 9] is now widely used for modelling of wheel-rail interactions [2, 6, 7, 8, 10]. Vehicle-track interaction studies in general consider track as a continuous system as Euler-Bernoulli [6, 7, 8] or Timoshenko beam [1, 2, 9, 10]. Most of these studies, however, represent vehicle by a rolling wheel to investigate the wheel-rail contact forces. The impact force response such as the bearing force, rail pad force, and the ballast force as well as the wheel-rail contact force in the presence of wheel flat utilizing comprehensive vehicle model is not available in literature. In addition to these, an in-depth investigation of the response of perfect wheel-rail contact point due to the adjacent wheel flat within the same axle is not studied. In the present paper, a dynamic computational model for the vehicle and track is formulated by means of modal analysis method. An idealized haversine wheel flat with the rounded corner is included in the wheel-rail contact model. The Rayleigh-Ritz method is employed to solve the coupled partial and ordinary differential equations of the vehicle-track system. A MATALB predefined code “ode45” has been employed to perform the time domain analyses of dynamic responses of the coupled system. The responses in terms of impact force of various vehicle and track components have been evaluated and analyzed.

2. VEHICLE AND TRACK SYSTEM MODEL

The vehicle system model used in this study consists of a quarter car supported on a bogie, while the side frame is supported on two wheelsets. The primary suspension connecting the wheels and the bogie frame is modeled as a parallel combination of a linear spring and a viscous damping element. The secondary suspension

connecting the bogie frame and the car body is also modeled by parallel spring and damping elements. The mass of the car body M_c, bogie mass M_t, wheel mass M_w are coupled through the suspension elements, as shown in Fig. 1. The vehicle is thus represented by a 5-DOF dynamic system that includes the car body vertical motion, $w_c(t)$; the bogie vertical and pitch motions, $w_t(t)$ and $\psi_t(t)$; and vertical motions of the wheels, $w_{w1}(t)$ and $w_{w2}(t)$. The primary suspension stiffness and damping elements are represented by K_{s1} and C_{s1}, respectively, while K_{s2} and C_{s2} represent the stiffness and viscous damping coefficient due to secondary suspension. The contact force at the leading wheel-rail and trailing wheel-rail are denoted by $P_1(t)$ and $P_2(t)$, respectively. J_t and $r(t)$ are mass moment of inertia of the bogie and wheel defect profile, respectively. l_f and l_r are the distance from the mass center of the bogie to the front and rear wheel centers, respectively. The motion of the rail beam coupled with the sleeper and ballast is expressed as $w_r(x,t)$, while $w_{si}(t)$ and $w_{bi}(t)$ describe the motions of the sleeper and ballast masses. K_p, C_p, K_b and C_b are the railpad and ballast stiffness and damping coefficients, respectively. K_w and C_w are the shear stiffness and damping coefficients of the ballast, respectively. The subgrade stiffness and damping are denoted as K_f and C_f, respectively. The rail mass per unit length is represented by m_r, M_s is mass of half of the sleeper and M_b is mass of each ballast block. In this study, 100 sleepers/ballasts are considered in order to ensure that there is no influence of rail end conditions. In general, 50 to 60 sleepers/ballast are considered sufficient for such study [8].

3. SYSTEM EQUATIONS OF MOTION

3.1 Equations of Vehicle

The equations of motion of the vehicle model are derived upon neglecting the contribution due to track roughness, while the contact forces developed at the wheel-rail interface are represented by $P_1(t)$ and $P_2(t)$. It is further assumed that the resultant secondary suspension force acts at the bogie mass center. The equations of motion of the vehicle system are summarized as:

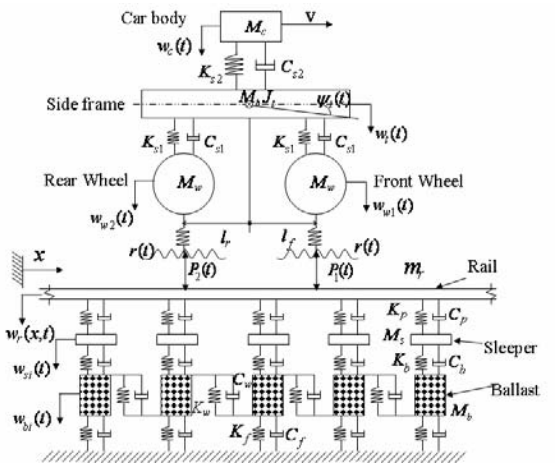

Fig.1: Vehicle and track system model

Car body bounce motion:

$$M_c\ddot{w}_c + C_{s2}\dot{w}_c + K_{s2}w_c - C_{s2}\dot{w}_t - K_{s2}w_t = 0 \quad (1)$$

Bogie bounce motion:

$$M_t\ddot{w}_t + K_{s1}(w_t + l_f\psi_t - w_{w1}) + K_{s1}(w_t - l_r\psi_t - w_{w2}) + K_{s2}(w_t - w_c) + C_{s1}(\dot{w}_t + l_f\dot{\psi}_t - \dot{w}_{w1}) + C_{s1}(\dot{w}_t - l_r\dot{\psi}_t - \dot{w}_{w2}) + C_{s2}(\dot{w}_t - \dot{w}_c) = 0 \quad (2)$$

Bogie pitch motion:

$$J_t\ddot{\psi}_t + K_{s1}l_f(w_t + l_f\psi_t - w_{w1}) - K_{s1}l_r(w_t - l_r\psi_t - w_{w2}) + C_{s1}l_f(\dot{w}_t + l_f\dot{\psi}_t - \dot{w}_{w1}) - C_{s1}l_r(\dot{w}_t - l_r\dot{\psi}_t - \dot{w}_{w2}) = 0 \quad (3)$$

Front wheel vertical motion:

$$M_w\ddot{w}_{w1} + C_{s1}(\dot{w}_{w1} - \dot{w}_t) + K_{s1}(w_{w1} - w_t) - C_{s1}l_f\dot{\psi}_t - K_{s1}l_f\psi_t + P_1(t) = 0 \quad (4)$$

Rear wheel vertical motion:

$$M_w\ddot{w}_{w2} + C_{s1}(\dot{w}_{w2} - \dot{w}_t) + K_{s1}(w_{w2} - w_t) + C_{s1}l_r\dot{\psi}_t + K_{s1}l_r\psi_t + P_2(t) = 0 \quad (5)$$

3.2 Equations of Rail Track

The equations of motion of the entire track system are derived upon integrating the equation of motion for the rail as an Euler beam with the differential equations of motions for the discrete sleeper and ballast supports. The deflection of the continuous rail can be derived from the partial differential equation for the Euler beam as [6]:

$$EI\frac{\partial^4 w_r(x,t)}{\partial x^4} + m_r\frac{\partial^2 w_r(x,t)}{\partial t^2} = -\sum_{i=1}^{N} F_{rsi}(t)\delta(x - x_i) + \sum_{j=1}^{2} P_j(t)\delta(x - x_j) \quad (6)$$

Where N is total number of sleepers considered in the model, k is the number of deflection modes considered for the rail beam and j is the number of wheelsets. E is the elastic modulus of rail beam materials and I is the second moment of area. The coordinate x represents the longitudinal position of the beam with respect to the left end support of the rail beam. x_i defines the position of the i th sleeper and $\delta(x)$ is the Dirac delta function.

$F_{rsi}(t)$ is the force developed at the i th rail/sleeper interface and given by:

$$F_{rsi}(t) = K_{pi}\left[w_r(x_i,t) - w_{si}(t)\right] + C_{pi}\left[\dot{w}_r(x_i,t) - \dot{w}_{si}(t)\right] \quad (7)$$

The term $P_j^{'}(t)$ in Eq. (6) defines the total vertical force acting at the j th wheel and rail interface. It comprises both the static vehicle load and the contact force $P_j(t)$, j =1, 2, such that:

$$P_j^{'}(t) = P_j(t) + [0.5(M_c + M_t) + M_w]g \;;\; j = 1, 2$$

The contact force $P_j(t)$ is derived using the Hertzian contact model described in section 3.3.

The equation of motion for the discrete sleeper and ballast masses are derived as follows:

$$M_{si}\ddot{w}_{si}(t) + (C_p + C_b)\dot{w}_{si}(t) + (K_p + K_b)w_{si}(t) - C_b\dot{w}_{bi}(t) - K_b w_{si}(t) - C_p\sum_{k=1}^{K} Y_k(x_i)\dot{q}_k(t) - K_p\sum_{k=1}^{K} Y_k(x_i)q_k(t) = 0 \;;\; i = 1, 2, ...N \quad (8)$$

$$M_{bi}\ddot{w}_{bi}(t) + (C_b + C_f + 2C_w)\dot{w}_{bi}(t) + (K_b + K_f + 2K_w)w_{bi}(t) - C_b\dot{w}_{si}(t) - K_b w_{si}(t) - C_w\dot{w}_{b(i+1)}(t) - K_w w_{b(i+1)}(t) - C_w\dot{w}_{b(i-1)}(t) - K_w w_{b(i-1)}(t) = 0 \;;\; i = 1, 2, ...N \quad (9)$$

3.3 Wheel-Rail Interaction

The wheel-rail contact has been widely described by the nonlinear Hertzian contact theory is commonly used for the wheel/rail interaction problems [1, 6, 8], which is also used in the present study. According to the Hertzian contact theory, the wheel-rail contact force is related to the rail deflection in a nonlinear manner, such that:

$$P(t) = C_H \Delta z(t)^{3/2} \quad (10)$$

Where $\Delta z(t)$ is the wheel-rail overlap in the vertical direction. In the presence of a wheel defect, the overlap is defined by the relative motion of the wheel with respect to the rail as:

$$[w_{wj}(t) - w_r(x_j,t) - r_j(t)] \;;\; j = 1, 2 \quad (11)$$

Where $r(t)$ is the wheel flat function. $w_w(t)$ and $w_r(x,t)$ are the wheel and rail deflections in vertical direction, respectively.

For a haversine flat, r is expressed as:

$$r = \frac{1}{2}D_f[1 - \cos(2\pi x / L_f)] \quad (12)$$

Where D_f is the flat depth, L_f is the length of the flat, x is the longitudinal coordinate of the contact point within the flat.

The contact force diminishes when a loss of contact of the wheel with the rail is encountered, when $[w_{wj}(t) - w_r(x_j,t) - r_j(t)] \le 0;\; j = 1, 2$

4. ANALYSIS METHOD

The track system model formulated in this study comprises both ODEs and PDE describing the deflection of the lumped sleeper and ballast masses, and the continuous rail, respectively. The PDE is expressed as ODEs by assuming a mode shape function. The Rayleigh-Ritz method is used to express the fourth order PDE describing the motion of the continuous rail by a series of second order ordinary differential equations in terms of the time coordinates. The resulting ODEs of the track and vehicle systems are than solved in time domain to obtained responses of individual components of the vehicle-track system model. The relative responses between the components are used to derive the dynamic interaction forces.

The deflection modes and the natural frequencies of an Euler beam in the absence of sleeper supports and external loads have been well documented and can be expressed as [6]:

$$Y_k(x) = \sin\left(\frac{k\pi x}{l}\right); \text{ and}$$

$$\omega_k = \left(\frac{k\pi}{l}\right)^2\sqrt{\frac{EI}{m_r}},\; k = 1, 2, 3\ldots K \quad (13)$$

Where is the deflection mode, ω_k is the corresponding natural frequency and l is the beam length.

The deflection response of the rail is then derived from :

$$w_r(x,t) = \sum_{k=1}^{K} Y_k(x)q_k(t) \quad (14)$$

Where K is the number of modes considered.

The substitution of the rail deflection response from Eq. (14) together with the mode shape Y_k in the PDE, Eq. (6) yields a set of ODEs in $q(t)$, expressed as:

$$\ddot{q}_k(t) + \alpha\sum_{i=1}^{N} C_{pi}Y_k(x_i)\sum_{k=1}^{K} Y_k(x_i)\dot{q}_k(t) + \frac{EI}{m_r}\left(\frac{k\pi}{l}\right)^4 q_k(t) + \alpha\sum_{i=1}^{N} K_{pi}Y_k(x_i)\sum_{k=1}^{K} Y_k(x_i)q_k(t) - \alpha\sum_{i=1}^{N} C_{pi}Y_k(x_i)\dot{w}_{si}(t) - \alpha\sum_{i=1}^{N} K_{pi}Y_k(x_i)w_{si}(t) = \alpha\sum_{j=1}^{2} P_j^{'}(t)Y_k(x_{Gj}) \quad (15)$$

Where $\alpha = (2/m_r l)$ and $k = 1, 2, 3\ldots\ldots\ldots K$

The equations of motion of the vehicle system described by Eqs. (1) to (5), and of the track system derived in Eqs. (6) to (9) together with the Hertzian nonlinear contact model in Eq. (10) describe the dynamics of the coupled vehicle-track system. Detail derivation of the vehicle-track model and method of analysis can be found in [11].

5. RESPONSE ANALYSES OF THE VEHICLE TRACK SYSTEM

The developed model is validated using the data reported by Zhai et al. [6]. In this reported study, a

10-DOF pitch plane model of the full car was considered with a three-layer Euler-Bernoulli beam track model to study the wheel-rail interaction due to a flat. The parameters for present simulation are taken from Zhai et al. [6], except for the primary suspension properties and Hertzian contact stiffness, which were not reported. These parameters were obtained for a typical wagon track system used in North America. The dynamic response of the entire vehicle-track system is evaluated under a constant speed of 27 km/h in the presence of a 52.8 mm long and 1 mm deep flat in the leading wheel. The time history of the dynamic contact force at the defective wheel-rail interface is compared with that reported in [6], as shown in Fig. 2. The results presented in Fig. 2 clearly show the effectiveness of the proposed quarter car vehicle model in predicting the contact force with the accuracy of a full vehicle model. This suggests negligible contributions due to the vehicle pitch, and a reduced model would be sufficient for accurately predicting the dynamic contact force due to a wheel flat.

The results in Fig.2 further show the sequence of events in terms of contact force and their frequency of oscillation, which can be explained in the following manner. As the wheel flat enters the contact area, there is a sudden drop in the contact force followed by a large peak due to the wheel-rail impact. This referred to as P1 force in literature [6], lasts for a short duration, which correspond to the duration of the flat in contact with the rail. The frequency of P1 can therefore be referred to as the excitation frequency due to the flat, and is a function of flat size and forward speed. The following sequence of peak force known as P2 force oscillates at a frequency of 125 Hz. This is primarily due to oscillation of the rail on the support pads. From various simulation runs, it is noticed that this frequency is unaffected by the flat size and speed, and is a function of pad properties. As shown in Fig. 2, the final sets of oscillation in wheel rail contact force takes place at a frequency of 56 Hz, which is attributed to the coupled vehicle-track natural frequency.

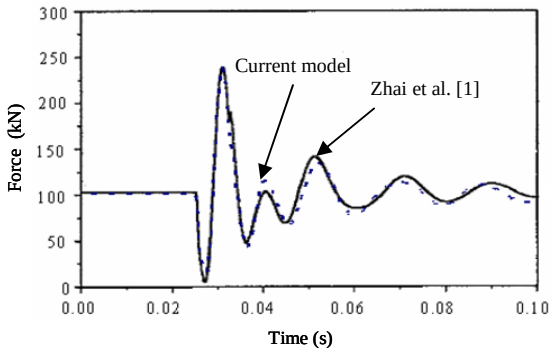

Fig 2: Comparison of wheel-rail impact force response of the present model with that reported by Zhai et al. [6].

Corresponding to a flat at the leading wheel, Fig. 3 shows the contact force response at flat-free rear wheel-rail contact point. The results clearly show significantly high contact force at the rear wheel-rail interface, even though the rear wheel is considered to be free of defects. For the flat size and speed considered, the peak contact force at the rear wheel reaches 1.62 times the static load while the peak impact force at the wheel with flat (Fig. 2) can reach 2.5 times the static load. The sequence of events at the rear wheel (Fig. 3) is somewhat different than that of the front wheel with flat (Fig. 2). This is attributed to the pitch motion of the bogie and phase difference between the motions of the wheel and rail at the front and rear axles.

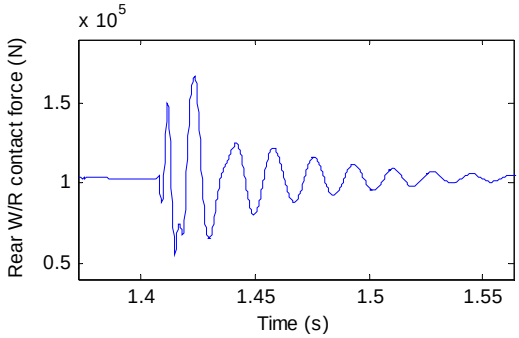

Fig 3: Time-history of impact force response at flat-free rear wheel-rail contact

These force time histories can be easily related to the wheel-rail displacement time histories presented in Fig. 4 (a) and 4 (b) for the defective and defect free wheels respectively.

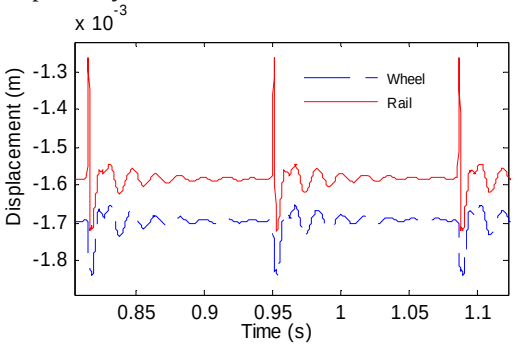

(a)

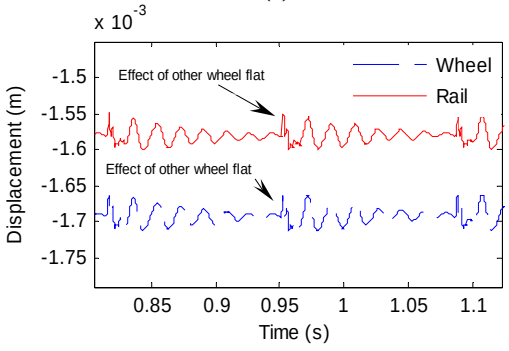

(b)

Fig 4: Wheel-rail displacement time history: (a) Defective wheel; (b) Defect-free wheel.

The validated vehicle-track system model is utilized to investigate the dynamic contact force at a constant forward speed of 70 km/h. The simulations are performed for a haversine wheel flat using the parameters presented in Table 1. The type of flat

considered closely meets the wheel removal criterion recommended by a number of American and European railroad organizations, such as Swedish Railway [2], AAR [12], Transport Canada [13] and UK Rail Safety and Standard Board [14].

Table 1: Simulation parameters

Symbol	Parameter	Value
M_c	Car body mass (quarter car)	19400 kg
M_t	Bogie mass	500 kg
M_w	Wheel mass	500 kg
J_t	Bogie mass moment inertia	176 kg-m^2
K_{s1}	Primary suspension stiffness	788 MN/m
C_{s1}	Primary suspension damping	3.5 kN-s/m
K_{s2}	Secondary suspension stiffness	6.11 MN/m
C_{s2}	Secondary suspension damping	158 kN-s/m
l_t	Wheelset distance	1.25 m
R	Wheel radius	0.42 m
L_f	Flat length	52 mm
D_f	Flat depth	0.4 mm
C_H	Hertzian spring constant	87 GN/m$^{3/2}$
m_r	Rail mass per unit length	60.64 kg/m
EI	Rail bending stiffness	6.62 MN-m^2
M_s	Sleeper mass	118.5 kg
M_b	Ballast mass	739 kg
K_p	Railpad stiffness	120 MN/m
K_b	Ballast stiffness	182 MN/m
K_w	Ballast shear stiffness	147 MN/m
K_f	Subgrade stiffness	78.4 MN/m
C_p	Railpad damping	75 kN-s/m
C_b	Ballast damping	58.8 kN-s/m
C_w	Ballast shear damping	80 kN-s/m
C_f	Subgrade damping	31.15 kN-s/m
l_S	Sleeper distance	0.6 m
N	No. of sleepers	100

The high magnitude contact forces developed at the wheel-rail interface are transmitted to the vehicle components and track layers, which may cause components fatigue or failure. The transmission of contact force to the sideframe occurs through the bearing adapters. The deflections of wheel and side frame give rise to the primary suspension force, also referred to as bearing force, which is eventually transmitted to the car body. The magnitudes of bearing forces strongly depend upon the nature of flat, speed, wheel load and suspension properties. The variations in bearing force are investigated using the baseline model for three different loading as shown in Fig. 5. The figure shows that the bearing force at the defective wheel follow the same trend as the impact force at the wheel-rail contact. The results further show that the peak bearing force at the bearing reaches 1.5, 1.73 and 1.93 times the static force for a 102, 82, 63 kN wheel loads, respectively. Corresponding to the above wheel loads, the wheel rail contact force was found to be 1.77, 1.96 and 2.45 times the static force.

The dynamic force developed by the discrete rail pads, also referred to as the reaction force at each rail-sleeper interface, is further evaluated to study the nature of forces transmitted to different track layers. The dynamic rail pad force is computed from relative deflection of the rail and sleeper, using Eq. (7). As an example, the variations in the rail pad force developed at sleeper no. 22, due to a flat within the rear wheel, are illustrated in Fig. 6.

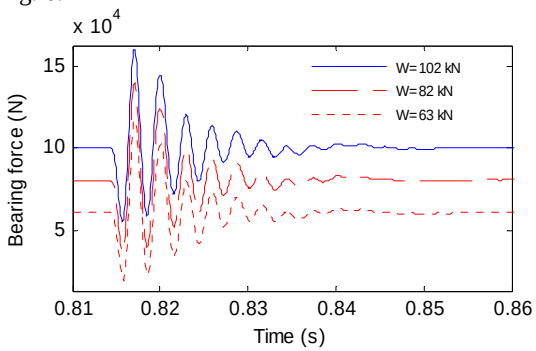

Fig 5: Variations in the bearing force response due to a rear-wheel flat as a function of static wheel load.

Figure 6 shows that as the wheel flat enters the wheel-rail contact region, the pad force first decreases from its static level. Similar to contact and bearing forces, the ratios of the peak pad force to static pad force are obtained as 1.46, 1.57, and 1.77 for static wheel load of 102, 82 and 63 kN, respectively. The figure further shows that the pad force gradually decreases after the impact, as the wheel moves away from the location of the sleeper. It can be seen that the variations in the wheel load do not influence the oscillation frequency of the pad force. The results also show that the magnitudes of pad forces are significantly smaller than those of the contact forces, which can be attributed to inertia force of the rail.

The impact force developed at wheel-rail interface due to a wheel flat is also transmitted to the ballast blocks, which is ultimately transmitted to the ground. The force developed at the sleeper-ballast interface is known as ballast force. The ballast force is computed by summing up the reaction forces obtained from a particular sleeper and the shear forces arising from couplings with the adjacent ballast blocks in the presence of a single flat in the rear wheel. The time

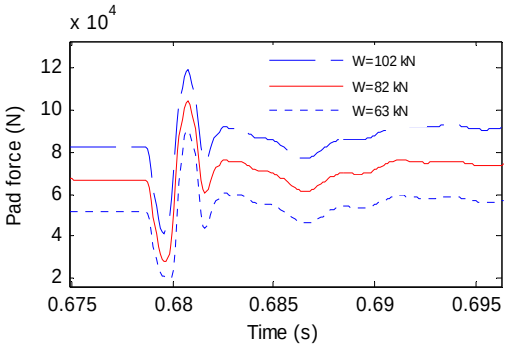

Fig 6: Variations in railpad force due to a rear wheel flat as a function of static wheel load.

histories of the ballast forces for ballast no. 22 under three different load conditions are shown in Fig. 7. The results suggest that variations in ballast forces are similar to those observed for the pad forces shown in Fig. 6. The peak magnitudes of the ballast forces, however, are considerably smaller than those of the pad forces. The ratios of peak to static ballast forces for wheel loads of 102, 82, and 63 kN are obtained as 1.32, 1.38, and 1.46, respectively. The normalized ballast forces are found to be relatively less sensitive to variations in the static wheel load in the range of variations considered. Comparison of ballast force results (Fig. 7) with pad force results (Fig. 6) clearly shows that the frequency of oscillation of the ballast force is significantly less than that of the pad force, while their trend is very similar.

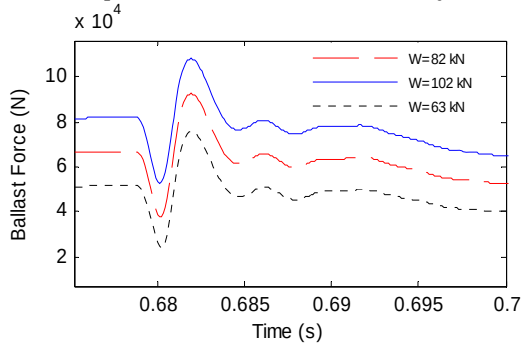

Fig 7: Variations in ballast force due to a rear wheel flat as a function of static wheel load.

6. DISCUSSIONS

The characteristics of the impact load due to a haversine wheel flat are investigated by a pitch plane vehicle model. The influence of the flat on various components of the vehicle and track is analyzed. This study illustrated the significant influence of wheel flat on the components of vehicle and track system. The current study also shows that flat present in one wheel has strong influence not only in wheel-rail impact forces but also on bearing, pad and ballast forces at the defective as well as adjacent wheelset. The investigations further show that the magnitudes of these transmitted forces as a ratio of static load could be significant and in general is lower for the lightly loaded wheel.

7. REFERENCES

1. Thompson, D., and Wu, T.X., "The effect of non-linearity on wheel/rail impact" Journal of Rail and Rapid transit, volume 218, part F, 2003, p1-15.
2. Sun, Y. Q., Dhanasekar, M., and Roach, D., "A three-dimensional model for the lateral and Vertical Dynamics of wagon-track system." Proceedings of the institution of Mechanical Engineers, Part F: Rail and Rapid Transit. Vol. 217 (1), 2003, p 31-45.
3. Hou, K., Kalousek, J., Dong, R., "A dynamic model for an asymmetrical vehicle/track system" Journal of Sound and Vibration 267 (2003) 591–604.
4. Knothe, K., and Grassie, S.L., "Modeling of railway track and vehicle/track interaction at high frequencies", Vehicle System Dynamics 22 1993, pp. 209 – 262.
5. Wen, Z., Jin, X., and Zhang, W., "Contact-impact stress analysis of rail joint region using the dynamic finite element method" Wear 258 (2005) p1301–1309.
6. Zhai, W. M., Cai, C. B., Wang, Q. C., Lu, Z.W., and Wu., X. S., "Dynamic Effects of Vehicles on Tracks in the Case of Raising Train Speed" Proceedings of the Institution of Mechanical Engineers, Part F, v 215, 2001, p125-135
7. Jin, X., Wen, Z., Wang, K., and Xiao, X., "Effect of passenger car curving on rail corrugation at a curved track" Volume 260, Issue 6, 10 March 2006, p619-633.
8. Zhai, W., and Cai, Z., "Dynamic interaction between a lumped mass vehicle and a discretely supported continuous rail track" Computers and Structures Vol. 63, No. 5, pp. 987-997, 1997.
9. Nielsen, J.C.O., and Oscarsson, J., "Simulation of dynamic train–track interaction with state-dependent track properties" Journal of Sound and Vibration, vol. 275 (2004) 515–532.
10. Sun, Y. Q., and Dhanasekar, M., "Importance of the track modeling on the determination of the critical speed of wagons" Vehicle system Dynamics Supplement 41 (2004), p232-241.
11. Rajib Ul Alam Uzzal, "Role of Railway Vehicle-Track System and Design Parameters on Flat-Induced Impact Load" M. A. Sc thesis, Dept. of Mechanical & Industrial Engineering, Concordia University, Montreal, Quebec, Canada 2007.
12. Lonsdale, C., Dedmon, S., and Pilch, J., "Effects of increased gross rail load on 36-inch diameter freight car wheels" available at www.standardsteel.com/rdpapers/2001
13. Transport Canada "Railway Freight Car Inspection and Safety Rules" available at http://www.tc.gc.ca/railway/Rules/TC_0-06-1.htm
14. Reilly, K., "Railway Wheelsets", Rail Safety and Standards Board, London, UK, June 2003.